SERS prospect of different organs from mouse and rat specimens exposed to UV radiation

A.Falamas[1,3], S. Pinzaru[1], C. Dehelean[2], Ch. Krafft[3], J. Popp[3,4]

1. Dept. of Physics, Babes Bolyai University, Kogalniceanu 1, RO 400084, Cluj-Napoca, România
2. Victor Babeş University of Medicine and Pharmacy, Faculty of Pharmacy, Eftimie Murgu Square 2, RO- 300041, Timişoara, România
3. Institute of Photonic Technology, Albert-Einstein-Straße 9, 07745, Jena, Germany
4. Institute of Physical Chemistry, Helmholtzweg 4, 07743, Jena, Germany

ABSTRACT

This study evaluates the capacity of infrared, Raman and surface enhanced Raman spectroscopy (SERS) to differentiate organs and to detect the structure and conformation of molecular components from healthy and cancerous tissues. Since most diseases are induced by biochemical processes including mutation and/or infection, they are accompanied by molecular composition changes in the tissues. Vibrational spectroscopy provides detailed information about the biomolecular composition of tissues, which might be used to distinguish between normal and malignant ones. The spectra of three organs (liver, lung and skin) from different specimens contain contributions from amino acids, proteins, lipids and cholesterol. The Raman spectra of normal skin are dominated by collagen, but also bands from lipids, DNA and the amide III and I bands of proteins. Raman images were collected to identify regions showing SERS effect and FTIR imaging was also applied as a complementary technique.

Sample preparation: 4 mice specimens – NMRI, C57 and Sprague Dawley – were exposed to UV radiation and DMBA (7,12-dymethilbenzanthracene) solution which was administered orally. Both treatments are known to induce cancer. Samples from lung, liver and skin were collected from each specimen and immersed in 10% formalin solution mixed with colloidal silver. Thin tissue sections were prepared and placed on CaF_2 slides.

Instrumentation: Single Raman spectra were collected from different regions from all samples placed on CaF_2 slides. Spectra were recorded using a Raman microscope coupled to a 785 nm diode laser (Kaiser Optical Systems). The laser power was set to 200 mW. The exposure time was 5 seconds and each spectrum was an average of 2 accumulations. Raman maps were acquired using the same instrument, each map having a dimension of 19 x 19 =361 spectra with a step size of 10 µm, exposure time 2 s per spectrum., number of acquisitions 2, dwell time between 10-30 s.

FTIR images were acquired in transmission mode using a FTIR microscopy coupled to a 64x64 focal plane array detector (Varian). 40 scans at 4 cm^{-1} resolution were collected and Fourier transformed to produce the resulting spectrum from 950 to 4000 cm^{-1}. Image dimension 350 x 350 μm^2.

Data analysis: The resulting Raman maps and FTIR images were processed using the CytoSpec software package. The data sets were normalized resulting in a linear correction of the complete spectrum , background subtraction, polynomial baseline correction. Low-intensity spectra were removed from the data sets because they corresponded to positions outside the tissue, near holes, near fissures or near margins. In FTIR images, the intensity of the amide I band near 1656 cm^{-1} was used to determine whether some regions of the sample were too thin for the spectra to be included in the subsequent data analysis, while in the Raman maps the 2750-3050 cm^{-1} interval was chosen.

Lung samples

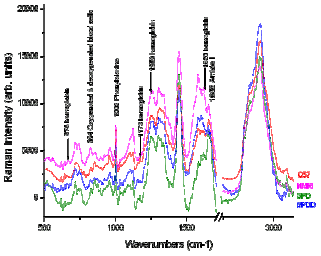

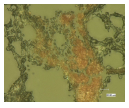

Macroscopic picture of lung sample showing high blood content. Picture acquired using a Keyence digital microscope

The high blood content of lungs gives enhanced Raman bands due to resonance effect at 675 (oxygenated cells symmetric pyrrole deformation), 824 (both oxygenated and deoxygenated cells methine out of plane deformation and pyrrole breathing mode), 973 (deoxygenated cells C-C asymmetric stretching of porphyrin macrocycle), 1124, 1171 (oxygenated cells asymmetric pyrrole half-ring stretching), 1250 (deoxygenated cells C-H methine deformation), 1370, 1561 and 1620 cm^{-1} upon 785 nm excitation => changes in the blood perfusion and in the red blood cells content can be easily detected by Raman spectroscopy.

FTIR imaging of lung NMRI sample

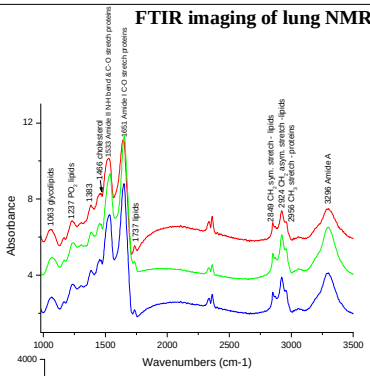

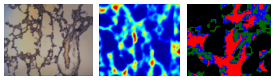

Microscopic picture of NMRI lung (10 x objective), IR imaging and HCA cluster analysis (from left) and the representative cluster-averaged IR spectra collected from tissue sections shown with the same color scale as in the pseudo color maps.

The IR spectra are dominated by the amide I and II band at 1653 and 1538 cm^{-1} which arise from the C=O stretching and N-H bending of the amide group, the CH_2 asymmetrical stretching mode of lipids at 2924 cm^{-1} and the amide A band at 3296 cm^{-1}.
FTIR imaging was applied as a complementary technique.

Raman mapping of lung sample from NMRI specimen

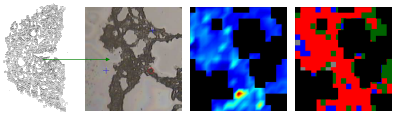

(from left) Microscopic picture of NMRI lung. Magnification 1.5, objective 1 x. Raman map of the selected area. The crosses delimit the dimension of the map (upper right and lower left). Distribution of the integrated intensity 2750-3050 cm^{-1}, hierarchical cluster analysis and the corresponding Raman spectra of the red, blue and green clusters.

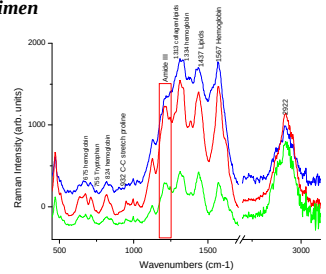

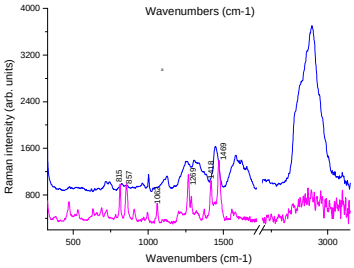

SERS effect (magenta spectrum) identified in the Raman map due to the Ag nanoparticles which penetrated the tissue, in comparison with a Raman spectrum recorded from the point next to it. The bands in the SERS spectrum are shifted towards smaller wavenumbers (717 Raman spectrum – 714 cm-1 SERS, indicating phospholipids, 1001 Raman spectrum -997 cm-1 SERS, assigned to phenylalanine). Other contributions observed in the SERS spectrum are lipids, proteins, heme groups, cholesterol, carotenoid and nucleic acdis to a lower extent

HCA analysis divided the tissue in 3 clusters, of which one (red spectrum) was assigned to the central part. Slight differences between the cluster averaged spectra showed that the concentration of proteins and lipids decreases when going from the tissue towards the margins. Contributions from hemoglobin are the most prominent and are present at 675, 748, 1334, 1370 and 1567 cm^{-1}. Significant differences can be seen in the interval 400-1800 cm^{-1} whereas the variances in the high wavenumber region are small.

Liver samples

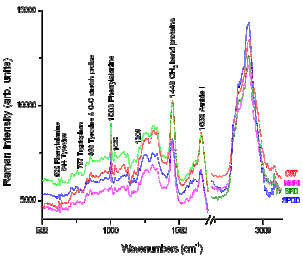

Raman spectra of liver tissues are dominated by contributions from proteins at 622 (phenylalanine), 644 (tyrosine), 757 (tryptophan), 853 (tyrosine and C-C stretching vibrations of proline), 1003, 1032 (phenylalanine), 1159 (C-C stretch of proteins), 1172 (C-H bend of tyrosine), 1209 (tryptophan and phenylalanine) and 1448 cm^{-1} (CH_2 bend of proteins), lipids and some influences from collagen and nucleic acids.

The spectra resemble very well and the only differences between specimens were found in the relative intensity of the present bands.

Skin samples

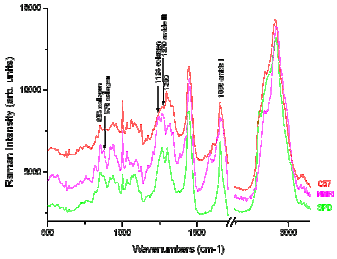

The major component in the Raman spectrum of normal skin is collagen, which can be identified by its characteristic Raman bands at 853, 876 and 1243 cm^{-1}. Further components are lipids, which can be localized in the stratum corneum or in the subcutis.

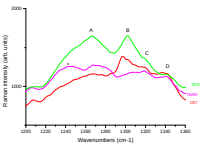

Raman spectra from 1200 to 1350 cm^{-1}. The indicated bands are: A - 1266 cm^{-1} amide III α-helix, B - 1302 cm^{-1} - CH_2 bend of lipids, C - 1319 cm^{-1} CH_3CH_2 wagging of collagen/lipids and D - 1336 cm^{-1} assigned to CH_3CH_2 wagging of collagen. The amide III band has decreased intensity in the NMRI and C57 spectra compared to the SPD spectrum.

The asterisk band present in NMRI spectrum at 1243 cm^{-1} distinctive for amide III collagen is missing in the red spectra and has a small contribution in the green one. The B band is nearly missing in the NMRI spectrum indicating a decrease in lipids.
Eczema is usually formed on dry skin so this can mean that Raman spectra should present a decrease in the lipids. Decreased intensity in the band at 1300 cm^{-1} in the NMRI spectrum has been correlated with skin after UV irradiation [4].
Raman spectrum of C57 specimen (red) shows an increased lipid content, which could be an indicator of skin with inflammatory disease.

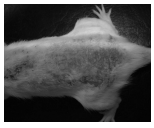

After exposure to ultraviolet radiation, the skin manifested injury in a variety of ways,including both acute and chronic responses, the most evident acute feature of UV radiation exposure being erythema (redness or sunburn).

NMRI specimen and conclusions

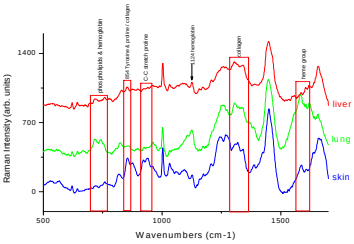

- In the graph to the right, Raman spectra from lung, liver and skin of NMRI specimen are presented. The Raman spectrum of skin is dominated by collagen, the liver spectrum is dominated by proteins and the lung spectrum is dominated by contributions from hemoglobin and proteins. **Comparing all three organs from the same specimen it is possible to identify the type of organ by analyzing the Raman bands present in the spectrum.**
- This study demonstrates **the capacity of Raman spectroscopy of differentiating between the same organ from distinct specimens** and the possibility of **identifying the structure and molecular components from healthy and diseased tissues.**
- Raman and FTIR imaging were applied to investigate areas from the tissues. In this way, **the SERS effect was identified**. This was expected due to the colloidal nanoparticles which were mixed with the formaline solution in which the samples were immersed. SERS spectra were acquired from normal and diseased organs **based on the Ag nanoparticles adsorbed in the tissue**.
- FTIR or Raman vibrational microspectroscopy can provide molecular information of samples with a high spatial resolution at microscopic level.
- Changes in specific cellular events such as an increase or decrease in substance classes (lipids, proteins, DNA) lead to differences in the Ramans and IR spectra.

Acknowledgment

We acknowledge financial support from the PN II – IDEI_2284, nr. 537/2008 grant from CNCSIS, Romania. One of the authors, A.F., highly acknowledges prof. Jürgen Popp and prof. Christoph Krafft from IPHT, Jena, for their support.

Selected References

1. Ch. Krafft, M. Kirsch, C. Beleites, G. Schackert and R. Salzer, *Methodology for fiber-optic Raman mapping and FTIR imaging of metastases in mouse brains*, Anal Bioanal Chem (2007) 389:1133–1142
2. R. E. Kast, G. K. Serhatkulu, A.Cao, *Raman Spectroscopy Can Differentiate Malignant Tumors from Normal Breast Tissue and Detect Early Neoplastic Changes in a Mouse Model*, Biopolymers, 81, 2007
3. Young-Kun Min, T. Yammamoto, E.Kohda, T.Ito and Hiro-o Hamaguchi, *1064 nm near-infrared multichannel Raman spectroscopy of fresh human lung tissues*, J. Raman Spectrosc. 2005; 36: 73–76
4. M. Gniadecka, O.F. Nielsen, S. Wessel, M. Heidenheim, D. H. Christensen, H. C. Wulf, *Water and protein structure in photoaged and chronically aged skin*, J. Investigative Dermatology, 1998, 111, 1129-1133